Emerging Two-Dimensional Conductivity at the Interface between Mott and Band Insulators

I. V. Maznichenko,[1,2,*] S. Ostanin,[1] D. Maryenko,[3,†] V. K. Dugaev,[4] E. Ya. Sherman,[5,6] P. Buczek,[2] I. Mertig,[1] M. Kawasaki,[3,7] and A. Ernst[8,9]

[1]*Institute of Physics, Martin Luther University Halle-Wittenberg, D-06099 Halle, Germany*
[2]*Department of Engineering and Computer Sciences, Hamburg University of Applied Sciences, Berliner Tor 7, D-20099 Hamburg, Germany*
[3]*RIKEN Center for Emergent Matter Science (CEMS), Wako 351-0198, Japan*
[4]*Department of Physics and Medical Engineering, Rzeszów University of Technology, 35-959 Rzeszów, Poland*
[5]*Department of Physical Chemistry and the EHU Quantum Center, University of the Basque Country UPV/EHU, Bilbao 48080, Spain*
[6]*Ikerbasque, Basque Foundation for Science, Bilbao, Spain*
[7]*Department of Applied Physics and Quantum-Phase Electronics Center (QPEC), The University of Tokyo, Tokyo 113-8656, Japan*
[8]*Institute for Theoretical Physics, Johannes Kepler University, A-4040 Linz, Austria*
[9]*Max Planck Institute for Microstructure Physics, Weinberg 2, D-06120 Halle, Germany*

(Received 18 September 2023; accepted 23 April 2024; published 21 May 2024)

Intriguingly, conducting perovskite interfaces between ordinary band insulators are widely explored, whereas similar interfaces with Mott insulators are still not quite understood. Here, we address the (001), (110), and (111) interfaces between the $LaTiO_3$ Mott, and large band gap $KTaO_3$ insulators. Based on first-principles calculations, we reveal a mechanism of interfacial conductivity, which is distinct from a formerly studied one applicable to interfaces between polar wideband insulators. Here, the key factor causing conductivity is the matching of oxygen octahedra tilting in $KTaO_3$ and $LaTiO_3$ which, due to a small gap in the $LaTiO_3$ results in its sensitivity to the crystal structure, yields metallization of its overlayer and following charge transfer from Ti to Ta. Our findings, also applicable to other Mott insulators interfaces, shed light on the emergence of conductivity observed in $LaTiO_3/KTaO_3$ (110) where the "polar" arguments are not applicable and on the emergence of superconductivity in these structures.

DOI: 10.1103/PhysRevLett.132.216201

The formation of a conducting layer at the interface between two insulators is one of the most intriguing problems in the physics of low dimensional electron systems. A remarkable example is the interface between two perovskite band insulators $LaAlO_3$ (LAO) and $SrTiO_3$ (STO) [1,2]. The electrons at such interface demonstrate high mobility, enabling the observation of the Shubnikov–de Haas oscillations and the quantum Hall effect [1,3,4]. Moreover, such interface can become superconducting, [5–8] possibly demonstrating unconventional Cooper pairing produced by the Rashba-like spin-orbit coupling.[9–16] The mechanism of two-dimensional electron gas (2DEG) formation is crucial for understanding emergent phenomena such as topological properties, quantum geometries, and superconductivity. [7,8,17–21]

For oxide electronics, the most prominent mechanism of the conductivity is the so called "polar catastrophe," broadly applicable to the (001)-oriented structures [22–34]. Here, $LaAlO_3$ is essentially thought to consist of oppositely charged layers $[LaO]^+$ and $[AlO_2]^-$, while the respective layers of $SrTiO_3$ are electrically neutral. The formation of a polar heterojunction $AlO_2/LaO/TiO_2$ eventually results in the electron transfer through the $LaAlO_3/SrTiO_3$ interface, which causes formation and filling of a conduction band formed by the Ti $3d$ electron states, responsible for conductivity and, at appropriate conditions, for superconductivity.

Recently, the isostructural perovskite $KTaO_3$ (KTO) attracted a lot of attention due to its ability to produce the surface superconducting state, strongly dependent on the crystal orientation [35–42]. Band insulator $KTaO_3$ can be brought in contact with Mott insulator $LaTiO_3$ (LTiO) epitaxially grown on its surface with emergence of a conducting LTiO/KTO interface [42]. Seemingly, it would be straightforward to consider the "polar catastrophe" as the mechanism of the 2DEG formation at the interface and the earlier studies for (001)-oriented LTiO/KTO found consistency with the mechanism [24]. This approach, however, fails to explain a highly conducting (110)-oriented interface that does not demonstrate the polar discontinuity. Moreover, the observed critical dependence of the interface superconductivity on the LTiO thickness [42] implies that the physics of this Mott insulator is one of the key factors responsible for the interface electronic

properties. Thus, another general mechanism of two-dimensional conductivity, possibly applicable to a variety of band-Mott insulator interfaces, is needed.

Here we use first-principles calculations to study the formation of interfacial conducting layers for (001), (110), and (111)-oriented LTiO/KTO heterojunctions. We demonstrate that the crystal structure effect, that is, the matching in the orientation of the oxygen octahedra surrounding Ti and Ta ions, at the interface and the following charge transfer across the interface are decisive for the formation of conducting layer. This mechanism resulting from a small gap in the LTiO, making it highly sensitive to the crystal structure variations, is distinct from the conventional explanation for polar band insulators and can be extended to other interfaces with Mott insulators.

To have reference points, we present the first-principles calculations of the bulk materials obtained with the Vienna Ab initio Simulation Package [43] within the Perdew-Burke-Ernzerhof generalized-gradient approximation [44] for the exchange-correlation potential and implementation of the lattice relaxation. (For technical details see Supplemental Material (SM) [45].) For a band insulator KTO, having the cubic unit cell with the experimental lattice constant $a_K = 3.989$ Å [49], this approach yields reliably wide gap while the calculated equilibrium volume overestimates slightly its experimental value by 2.3%. The calculated band gap between Ta $5d$ and O p states exceeds 2 eV.

Calculation of the bulk Mott insulator LTiO within the density functional theory (DFT) needs the DFT + U parametrization [50,51], i.e., the appropriate correlation parameter U applied to the $3d$ orbitals of Ti. This orthorhombic material with lattice parameters $a_L = b_L = 5.595$ Å and $c_L = 7.912$ Å has a pseudocubic structure with the lattice constant $a_{pc} = a_L/\sqrt{2} = c_L/2 = 3.956$ Å, different by only 0.8% from the a_K of the cubic KTO. This structure is characterized by the tilting angle $\theta = 180° - \angle BOB$ (here $B =$ Ti), defined as the deviation from the cubic perovskite structure ABO_3, with the experimental value $\theta = 26°$. The Vienna Ab initio Simulation Package implementation [52] with the effective $U_{eff} = 2.3$ eV gives for orthorhombic ($Pbnm$) LTiO (i) the band gap of 0.5 eV, (ii) the G-type antiferromagnetic structure, and (iii) the Ti magnetic moment of 0.7 μ_B, in agreement with other numerical approaches [53,54]. This small 0.5 eV band gap makes the LTiO very sensitive to perturbations and, as we will see, can result in the formation of the 2DEG at the LTiO/KTO interface. To simulate LTiO/KTO (001) interfaces we constructed superlattice from the 8-f.u.-thick (f.u. for formula unit) KTO (001) and 8-f.u.-thick LTiO (001) using the experimental lattice parameters of LTiO for the in-plane geometry. For the LTiO/KTO (110) interface, we used mainly a 240-atom 8-f.u.-LTiO/4-f.u.-KTO supercell, which contains four f.u. of ABO_3 perovskite in each layer. The (111) interface was simulated using a 160-atom LTiO/KTO supercell, where each atomic layer contains the two f.u. of ABO_3.

Considering epitaxial interfaces of materials with different lattices, one expects a local modification increasing their similarity, within several atomic layers near the interface. Various structural alterations in similar structures were discussed in experimental and theoretical studies [55–61], but the tilting of oxygen octahedra has never been considered as the main source for 2DEG formation. However, for small gap materials such as LTiO, this local modification can lead to a sufficient alteration of the electron bands. Since the principal difference between KTO and LTiO is the tilting of the oxygen octahedra, we expect a certain matching of the octahedra tiltings near the interfaces. To clearly show the sensitivity to perturbations in terms of the octahedra tilting, we begin with a computer experiment by calculating the hypothetical cubic $LaTiO_3$ without TiO_6 tilting. As this realization is metallic, as shown in the Supplemental Material, we see that the key *lattice structural* factor of strongly correlated LTiO, keeping its finite small band gap and antiferromagnetism, is the tilting.

To quantitatively understand the critical impact of the tilting on the electronic structure and 2DEG formation, we calculate the bulk electronic and magnetic properties of KTO and LTiO at discrete tilting angles without the following relaxation.

Figure 1 shows the band gap of KTO and LTiO [panel (a)] and its total energy [panel (b)] calculated as a function of θ. With decreasing θ the LTiO Mott gap decreases and closes for $\theta < 20°$. Thus, a small decrease

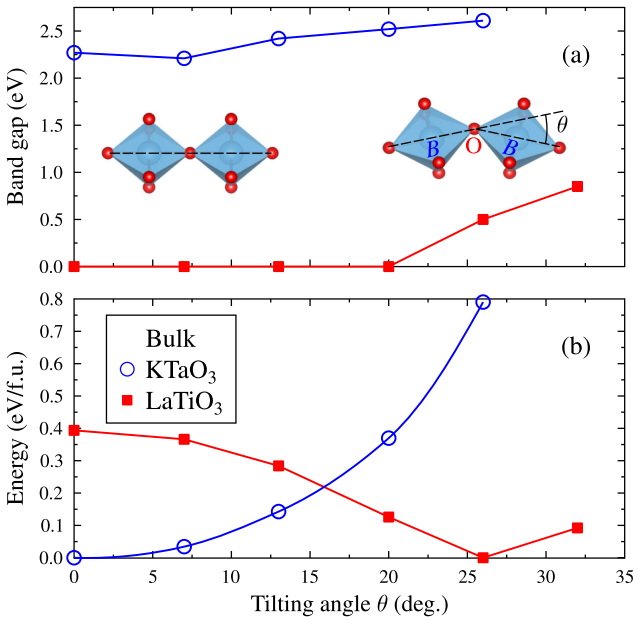

FIG. 1. The band gap (a) and total energy (b) of orthorhombic KTO and LTiO as a function of the tilting angle θ. Inset in panel (a) provides definition of the tilting angle $\theta = 180° - \angle BOB$, where $B =$ Ta and $B =$ Ti for KTO and LTiO, respectively. Energies are calculated with respect to the energies with the equilibrium optimally tilted $\theta = 0$ for KTO and $\theta = 26°$ for LTiO.

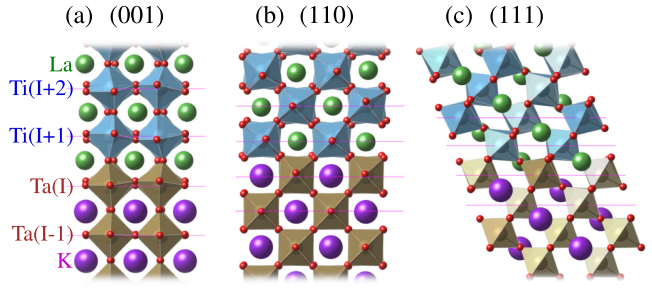

FIG. 2. Interfacial LTiO/KTO configurations of the (001), (110), and (111) heterojunctions, which are plotted in the (a), (b), and (c) panels, respectively. La is shown in green, K in magenta, O in red. The TaO_6 and TiO_6 octahedra are shown in brown and blue, respectively. A tilting of octahedra is clear to see for TiO_6 in LTiO and for interfacial TaO_6 in KTO. The distances between planes are $a_{pc}/2 \approx 2$ Å, $a_{pc}/(2\sqrt{2}) \approx 1.4$ Å, and $a_{pc}/(2\sqrt{3}) \approx 1.2$ Å for (001), (110), and (111), respectively.

in θ with respect to its experimental value in LTiO provokes the insulator-to-metal transition. For a wideband insulator such as KTO or LAO, for comparison, the variation in θ does not affect significantly the wide gap value. The total energy of LTiO [Fig. 1(b)] shows that robustly metallic LTiO calculated without tilting ($\theta = 0$) is unfavorable by 0.4 eV per the formula unit as compared to the optimally tilted LTiO. We found also that the Ti magnetic moments decrease gradually with decreasing θ to completely nonmagnetic Ti sites in untilted LTiO. The spin-polarized density of states (DOS) of untilted bulk LTiO is presented in the SM [45] illustrating that this phase is metallic with E_F being about 0.8 eV above the conduction band edge. Thus, if, for certain reasons, the tilting angle in LTiO at the interface decreases compared to the bulk structure, this can cause the 2DEG formation and can be referred to as the "undertilting" mechanism of emergence of the conductivity.

We begin with a formal description of the interfaces based on ionic charges. Figure 2 presents the interfacial region of the calculated (001), (110), and (111) LTiO/KTO structures, respectively. Among the three interfaces, only the (110) one is unpolar (see Table I).

TABLE I. Plane charge sequence and in-plane magnetic order for three interface orientations. Numbers show the nominal charge for planes ("//" denotes the interface). Note that the sequence is continuous only for the (110) interface meaning that the polarity-based arguments are not applicable there. The magnetic ordering (AFM for antiferromagnetic, FM for ferromagnetic) corresponds to cross sections of the bulk LTiO by the planes with the corresponding orientations.

Interface	Plane charge sequence	In-plane magnetic order
(001)	$-1/+1/-1/+1//+1/-1/+1/-1$	AFM chessboard
(110)	$-4/+4/-4/+4//-4/+4/-4/+4$	AFM chains
(111)	$-5/+5/-5/+5//-3/+3/-3/+3$	FM

In our main task we study the LTiO/KTO interfaces with first principle calculations. The key feature of the obtained optimized atomic positions and the crystalline structure at the interfaces is the strong layer dependence of the tilting angles θ on both LTiO and KTO sides for all considered orientations. Figure 3 shows the calculated tilting angles θ plotted as a function of the supercell z coordinate. Although the z dependence of θ varies from orientation to orientation, as seen in Fig. 3, the calculations demonstrate that θ strongly decreases in LTiO toward the interface for all of them. The minimization of the lattice energy tends to match the orientation of the oxygen octahedra in KTO and LTiO at the interface producing KTO-related tilting up to 10° in its interfacial unit cells. Thus, the weak tilting of the oxygen octahedra in LTiO interfacial layers, insufficient to form the Mott insulator, leads to its metallization and formation of the 2DEG at all these interfaces.

Now we consider this interface-based 2DEG in detail. For all considered orientations of interfaces, we found that it is formed mainly by the B-type cations, Ta and Ti, placed in the two interfacial unit cells of KTO and LTiO with the spin-polarized DOS calculated for Ta and Ti in the interfacial layers I and $I+1$ presented in Fig. 4. To compare the $3d$ Ti and $5d$ Ta contributions for the three 2DEGs, we calculated for Ta(I) and Ti($I+1$) the integrated DOS from the conduction band bottom to the Fermi energy E_F. The corresponding charges q, which are presented in Table II, show that in LTiO/KTO (001) each interfacial Ta-Ti pair contributes exactly one electron to its 2DEG. Thus, the interface (001) simply closes the gap and transfers the q portion of 1/3 from Ti($I+1$) to Ta(I). In LTiO/KTO (110) and LTiO/KTO (111), $q[\mathrm{Ta}(I)] + q[\mathrm{Ti}(I+1)]$ increases to 1.24 and 1.75, respectively. This can be attributed to the increased density of states and to the changes in the number of atomic neighbors, with Ta(I) having one, two, and

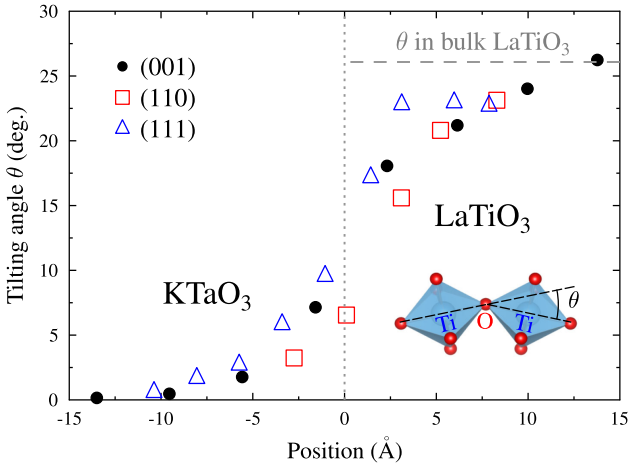

FIG. 3. Variation of the tilting angles in LTiO/KTO (001), (110), and (111) interfaces after relaxation. Vertical dashed line accords to z coordinate of the interfacial atom Ta (I). Inset corresponds to Fig. 1(a).

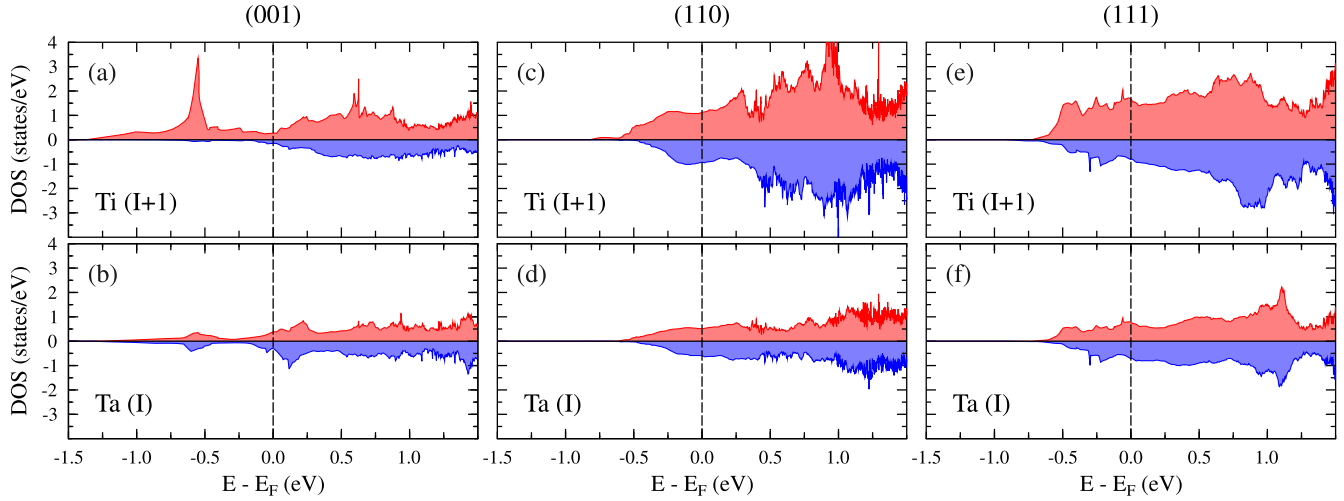

FIG. 4. Spin-polarized DOS calculated for the interfacial Ti and Ta in LTiO/KTO interfaces: (001), (a) and (b); (110), (c) and (d); (111), (e) and (f), respectively.

three Ti$(I+1)$ neighbors at the (001), (110), and (111) interface, respectively. For all the interfaces, occupations of Ta and Ti sites are mutually related due to the common Fermi energy for all electron sub-bands and the state hybridization. It is interesting to mention that the calculations show the charge ratio $q[\mathrm{Ta(I)}]/q[\mathrm{Ti(I+1)}] \approx 0.5$ for all of the interfaces.

The DOS at the Fermi level of the order of 1 state/eV and charges $q[\mathrm{Ta(I)}] + q[\mathrm{Ti(I+1)}]$ correspond to a typical metal with the density of the order of one electron per unit cell, in agreement with the experiment [24,42]. For the (110) and (111) interfaces the DOS at the Fermi level is significantly larger than that at the (001) interface; see Table II. This difference, which for the (110) interface can be attributed to the anisotropy of the Fermi surface, agrees with the absence of superconductivity in the (001) heterostructures [42]. Indeed, in the BCS-based approaches the superconducting transition temperature critically depends on the product of the DOS at the Fermi level and the coupling constant of effective electron-electron attraction. Although this constant and its dependence on the interface geometry are unknown at the moment, low Fermi level DOS hints at suppressed formation of Cooper pairs provided that the coupling constant does not strongly depend on the interface orientation.

TABLE II. Effective charges q (in the units of electron charge) corresponding to the 2DEG at LTiO/KTO interfaces, projected at the interfacial Ta and Ti, and corresponding density of states at Fermi level n_F.

Interface	$q[\mathrm{Ta}(I)]$	$q[\mathrm{Ti}(I+1)]$	$n_F[\mathrm{Ta}(I)]$	$n_F[\mathrm{Ti}(I+1)]$
(001)	0.32	0.67	0.68	0.43
(110)	0.39	0.85	1.10	2.03
(111)	0.58	1.17	1.52	2.40

The lower density of states can be attributed to larger interlayer distances in LTiO/KTO (001) heterostructure. This reduces hybridization via the interface, which is reflected in the DOS: the ferromagnetic highly spin-polarized peak at ≈0.6 eV below the Fermi level [see Figs. 4(a),(b)] corresponding to narrow bands of correlated Ti-based electrons, includes many electron states. Since it pulls electrons below the Fermi level and, thus, decreases the corresponding density of states at the Fermi level as expected for the (001)-related symmetry. In addition to the charge transfer, the proximity with the highly polarized Ti$(I+1)$ magnetic moments induces a weak spin polarization of neighboring Ta with the magnetic moments of the interfacial Ta(I) being about 0.06 μ_B (see Sec. III in SM for analysis of atomic configurations at interfaces [45]).

The very similar shapes of their site-projected DOS and similar numerical values, show that the metallization involves Ti and Ta atoms contributions on the same scale, with $5d$ of Ta states getting a considerable population and becoming conducting together with the contribution of Ti electrons. Thus, the origin of the 2DEG in these systems is different from the case of the LAO/STO (001) interface, in which the 2DEG is formed with the interface polarity accompanied by corresponding band bending.

In Fig. 5 each panel shows the energy branches associated with the d states of Ta or Ti near the interface. The lowest $E(\mathbf{k})$ branches of LTiO/KTO (001), which form its conduction band edge, E_C, belong to the interfacial Ta(I), as Fig. 5(b) shows. Figures 5(a) and 5(b) show the upshift of the bottom of the corresponding conduction band from Ta(I) to Ta(I-1) layer by approximately 1 eV, indicating a very strong band bending effect, common with the LAO/STO (001). For comparison, the branches of interfacial Ti$(I+1)$ and the next to it Ti$(I+2)$ appear at approximately the same energies, meaning a much weaker band bending effect on this side of the interface, as can be seen in

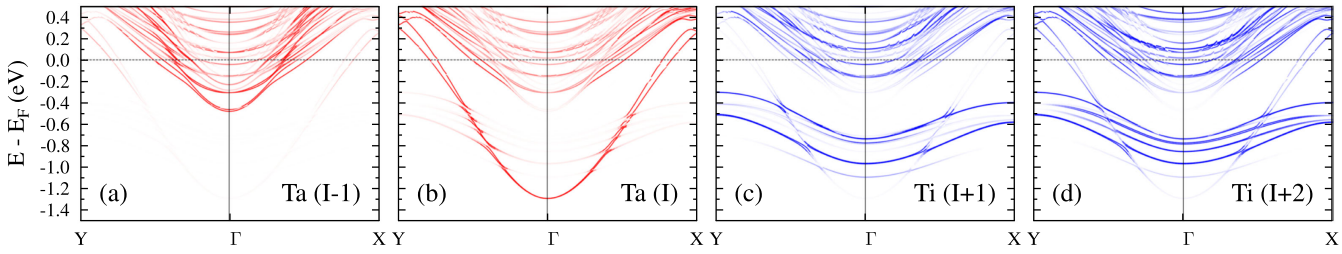

FIG. 5. The 2DEG band structure associated with interfacial Ta and Ti in LTiO/KTO (001) with the notations defined in Fig. 2. The large density of Ti-based bands at $E - E_F \approx -0.6$ eV corresponds to the peak in the density of states in this energy range as presented in Fig. 4. The intensity of the lines corresponds to the contribution of the given atom in the band state.

Figs. 5(c) and 5(d). No significant band bending was numerically found at the LTiO/KTO (110) and (111) interfaces. Comparison of Figs. 5(a)–5(d) shows that 2DEG at the LTiO/KTO (001) interface is formed by three different kinds of electron bands: (i) broad Ta-based bands weakly hybridized with the Ti-based ones, demonstrating a considerable band banding and contributing to the formation of the 2DEG; (ii) a large number of narrow Ti-based bands, not crossing the Fermi level, weakly hybridized with the Ta-based ones; and (iii) a large number of considerably hybridized Ti and Ta-based bands crossing the Fermi level. The two latter kinds of bands do not show a strong bending pattern.

Summarizing, the (001), (110), and (111) crystal interfaces between the polar materials such as Mott insulator $LaTiO_3$ and wideband $KTaO_3$ were simulated from the first principles. For all three interfaces we found that their calculated metallic densities of states, formed mostly by the interfacial Ti $3d$ and Ta $5d$ states, qualitatively agree with the experimental results. One of key reasons for the formation of two-dimensional metals in all these systems is a strong altering of the oxygen octahedra tilting angles at the interfaces, matching their orientation in KTO and LTiO and considerably decreasing it at the LTiO side compared to the corresponding bulk value. This "undertilting" destroys the small LTiO Mott-like band gap at all interfaces (see Figs. 1 and 3), making it the qualitative feature for these systems. At the (001) and (111) interfaces this mechanism can work together with the polarity-induced interface charge transfer making these two effects involving interacting electrons and lattice distortion inseparable. However, it is important to stress that the appearance of the conducting electrons at the (110) interface cannot be attributed to the polarity (see Table I) effects and, therefore, the "undertilting" is critically important for the conductivity and, at appropriate conditions, for the superconductivity, of this heterostructure. We note that the relatively high density of states of the conducting electrons at the (110) and (111) interfaces can be the decisive factor of their superconductivity in contrast to the (001) interface, which is metallic but not superconducting. Another factor that can be detrimental for superconductivity at the (001) interface is the ferromagnetic behavior of interfacial electron states shown in Fig. 4(a). The role of local defects in the 2DEG formation was not considered in our calculations since for the obtained 2DEG at the entire interface area with a large electron concentration and the density of states, a weak disorder in high-quality structures is a marginal effect [32–34,42].

To provide an outlook and further development of this research, we stress that the proposed picture of formation of two-dimensional conducting systems of interacting electrons can be applied to various interfaces between wide gap and small gap perovskite Mott insulators. To make this picture applicable, the interface structure should favor tilting of the oxygen octahedra different from that in the bulk Mott insulator with its band structure being strongly sensitive to the tilting, as possibly can occur for thin films of $LaVO_3$ grown on $SrTiO_3$ substrates [23,62].

A. E. acknowledges funding by Fonds zur Förderung der Wissenschaftlichen Forschung (FWF) Grant No. I 5384. The work of E. S. is financially supported through Grant No. PID2021-126273NB-I00 funded by MCIN/AEI/10.13039/501100011033 and by ERDF "A way of making Europe," and by the Basque Government through Grant No. IT1470-22. The work of M. K. was supported by JSPS KAKENHI (22H04958).

*Corresponding author: igor.maznichenko@physik.uni-halle.de
†Corresponding author: maryenko@riken.jp

[1] A. Ohtomo and H. Y. Hwang, Nature (London) **427**, 423 (2004).
[2] S. Thiel, G. Hammerl, A. Schmehl, C. W. Schneider, and J. Mannhart, Science **313**, 1942 (2006).
[3] A. McCollam, S. Wenderich, M. K. Kruize, V. K. Guduru, H. J. A. Molegraaf, M. Huijben, G. Koster, D. H. A. Blank, G. Rijnders, A. Brinkman, H. Hilgenkamp, U. Zeitler, and J. C. Maan, APL Mater. **2**, 022102 (2014).
[4] F. Trier, G. E. D. K. Prawiroatmodjo, Z. Zhong, D. V. Christensen, M. von Soosten, A. Bhowmik, Juan Maria Garcia Lastra, Y. Chen, T. S. Jespersen, and N. Pryds, Phys. Rev. Lett. **117**, 096804 (2016).
[5] N. Reyren, S. Thiel, A. D. Caviglia, L. F. Kourkoutis, G. Hammerl, C. Richter, C. W. Schneider, T. Kopp,

A.-S. Rüetschi, D. Jaccard, M. Gabay, D. A. Muller, J.-M. Triscone, and J. Mannhart, Science **317**, 1196 (2007).
[6] A. D. Caviglia, S. Gariglio, N. Reyren, D. Jaccard, T. Schneider, M. Gabay, S. Thiel, G. Hammerl, J. Mannhart, and J.-M. Triscone, Nature (London) **456**, 624 (2008).
[7] L. Li, C. Richter, J. Mannhart, and R. C. Ashoori, Nat. Phys. **7**, 762 (2011).
[8] J. A. Bert, B. Kalisky, C. Bell, M. Kim, Y. Hikita, H. Y. Hwang, and K. A. Moler, Nat. Phys. **7**, 767 (2011).
[9] A. D. Caviglia, M. Gabay, S. Gariglio, N. Reyren, C. Cancellieri, and J.-M. Triscone, Phys. Rev. Lett. **104**, 126803 (2010).
[10] M. Ben Shalom, M. Sachs, D. Rakhmilevitch, A. Palevski, and Y. Dagan, Phys. Rev. Lett. **104**, 126802 (2010).
[11] Y. A. Bychkov and E. I. Rashba, J. Phys. C **17**, 6039 (1984).
[12] J. W. F. Venderbos, L. Savary, J. Ruhman, P. A. Lee, and L. Fu, Phys. Rev. X **8**, 011029 (2018).
[13] L. P. Gor'kov and E. I. Rashba, Phys. Rev. Lett. **87**, 037004 (2001).
[14] M. S. Scheurer and J. Schmalian, Nat. Commun. **6**, 6005 (2014).
[15] V. Kozii and L. Fu, Phys. Rev. Lett. **115**, 207002 (2015).
[16] S. Nakosai, Y. Tanaka, and N. Nagaosa, Phys. Rev. Lett. **108**, 147003 (2012).
[17] A. Joshua, J. Ruhman, S. Pecker, E. Altman, and S. Ilani, Proc. Natl. Acad. Sci. U.S.A. **110**, 9633 (2013).
[18] D. C. Vaz, P. Noël, A. Johansson, B. Göbel, F. Y. Bruno, G. Singh, S. Mckeown-Walker, F. Trier, L. M. Vicente-Arche, A. Sander *et al.*, Nat. Mater. **18**, 1187 (2019).
[19] E. Lesne, Y. G. Sağlam, R. Battilomo, M. T. Mercaldo, T. C. van Thiel, U. Filippozzi, C. Noce, M. Cuoco, G. A. Steele, C. Ortix, and A. D. Caviglia, Nat. Mater. **22**, 576 (2023).
[20] A. Gao *et al.*, Science **381**, 181 (2023).
[21] N. Wang, D. Kaplan, Z. Zhang, T. Holder, N. Cao, A. Wang, X. Zhou, F. Zhou, Z. Jiang, C. Zhang, S. Ru, H. Cai, K. Watanabe, T. Taniguchi, B. Yan, and W. Gao, Nature (London) **621**, 487 (2023).
[22] N. Nakagawa, H. Y. Hwang, and D. A. Muller, Nat. Mater. **5**, 204 (2006).
[23] Y. Hotta, T. Susaki, and H. Y. Hwang, Phys. Rev. Lett. **99**, 236805 (2007).
[24] K. Zou, S. Ismail-Beigi, K. Kisslinger, X. Shen, D. Su, F. J. Walker, and C. H. Ahn, APL Mater. **3**, 036104 (2015).
[25] J. Biscaras, N. Bergeal, A. Kushwaha, T. Wolf, A. Rastogi, R. Budhani, and J. Lesueur, Nat. Commun. **1**, 89 (2010).
[26] P. Moetakef, T. A. Cain, D. G. Ouellette, J. Y. Zhang, D. O. Klenov, A. Janotti, C. G. Van de Walle, S. Rajan, S. J. Allen, and S. Stemmer, Appl. Phys. Lett. **99**, 232116 (2011).
[27] A. H. Al-Tawhid, D. P. Kumah, and K. Ahadi, Appl. Phys. Lett. **118**, 192905 (2021).
[28] J. Goniakowski, F. Finocchi, and C. Noguera, Rep. Prog. Phys. **71**, 016501 (2008).
[29] H. Chen, A. M. Kolpak, and S. Ismail-Beigi, Adv. Mater. **22**, 2881 (2010).
[30] N. C. Bristowe, P. Ghosez, P. B. Littlewood, and E. Artacho, J. Phys. Condens. Matter **26**, 143201 (2014).
[31] S. Stemmer and S. J. Allen, Annu. Rev. Mater. Res. **44**, 151 (2014).
[32] I. V. Maznichenko, S. Ostanin, V. Dugaev, I. Mertig, and A. Ernst, Phys. Rev. Mater. **2**, 074003 (2018).
[33] I. V. Maznichenko, S. Ostanin, A. Ernst, and I. Mertig, Phys. Rev. Mater. **3**, 074006 (2019).
[34] I. V. Maznichenko, S. Ostanin, A. Ernst, J. Henk, and I. Mertig, Phys. Status Solidi (b) **257**, 1900540 (2020).
[35] K. Ueno, S. Nakamura, H. Shimotani, H. T. Yuan, N. Kimura, T. Nojima, H. Aoki, Y. Iwasa, and M. Kawasaki, Nat. Nanotechnol. **6**, 408 (2011).
[36] C. Liu, X. Yan, D. Jin, Y. Ma, H.-W. Hsiao, Y. Lin, T. M. Bretz-Sullivan, X. Zhou, J. Pearson, B. Fisher, J. S. Jiang, W. Han, J.-M. Zuo, J. Wen, D. D. Fong, J. Sun, H. Zhou, and A. Bhattacharya, Science **371**, 716 (2021).
[37] Z. Chen, Y. Liu, H. Zhang, Z. Liu, H. Tian, Y. Sun, M. Zhang, Y. Zhou, J. Sun, and Y. Xie, Science **372**, 721 (2021).
[38] Z. Chen, Z. Liu, Y. Sun, X. Chen, Y. Liu, H. Zhang, H. Li, M. Zhang, S. Hong, T. Ren, C. Zhang, H. Tian, Y. Zhou, J. Sun, and Y. Xie, Phys. Rev. Lett. **126**, 026802 (2021).
[39] C. Liu, X. Zhou, D. Hong, B. Fisher, H. Zheng, J. Pearson, J. S. Jiang, D. Jin, M. R. Norman, and A. Bhattacharya, Nat. Commun. **14**, 951 (2023).
[40] X. Hua, F. Meng, Z. Huang, Z. Li, S. Wang, B. Ge, Z. Xiang, and X. Chen, npj Quantum Mater. **7**, 97 (2022).
[41] E. G. Arnault, A. H. Al-Tawhid, S. Salmani-Rezaie, D. A. Muller, D. P. Kumah, M. S. Bahramy, G. Finkelstein, and K. Ahadi, Sci. Adv. **9**, eadf1414 (2023).
[42] D. Maryenko, I. Maznichenko, S. Ostanin, M. Kawamura, K. Takahashi, M. Nakamura, V. Dugaev, E. Y. Sherman, A. Ernst, and M. Kawasaki, APL Mater. **11**, 061102 (2023).
[43] G. Kresse and J. Furthmüller, Phys. Rev. B **54**, 11169 (1996).
[44] J. P. Perdew, K. Burke, and M. Ernzerhof, Phys. Rev. Lett. **77**, 3865 (1996).
[45] See Supplemental Material at http://link.aps.org/supplemental/10.1103/PhysRevLett.132.216201 which includes Refs. [47–49], for technical details and electronic properties of bulk.
[46] D. Hobbs, G. Kresse, and J. Hafner, Phys. Rev. B **62**, 11556 (2000).
[47] H. L. Meyerheim, F. Klimenta, A. Ernst, K. Mohseni, S. Ostanin, M. Fechner, S. Parihar, I. V. Maznichenko, I. Mertig, and J. Kirschner, Phys. Rev. Lett. **106**, 087203 (2011).
[48] R. Guo, L. Tao, M. Li, Z. Liu, W. Lin, G. Zhou, X. Chen, L. Liu, X. Yan, H. Tian, E. Y. Tsymbal, and J. Chen, Sci. Adv. **7**, eabf1033 (2021).
[49] A. Tkach, P. M. Vilarinho, and A. Almeida, J. Eur. Ceram. Soc. **31**, 2303 (2011).
[50] V. I. Anisimov, J. Zaanen, and O. K. Andersen, Phys. Rev. B **44**, 943 (1991).
[51] J. Varignon, M. Bibes, and A. Zunger, Nat. Commun. **10**, 1658 (2019).
[52] A. Rohrbach, J. Hafner, and G. Kresse, J. Phys. Condens. Matter **15**, 979 (2003).
[53] H.-S. Ahn, D. D. Cuong, J. Lee, and S. Han, J. Korean Phys. Soc. **49**, 1536 (2006).
[54] J. Varignon, M. Bibes, and A. Zunger, Phys. Rev. B **100**, 035119 (2019).

[55] H. Ishida and A. Liebsch, Phys. Rev. B **77**, 115350 (2008).
[56] S. Okamoto and A. J. Millis, Nature (London) **428**, 630 (2004).
[57] J.-L. Maurice, C. Carrétéro, M.-J. Casanove, K. Bouzehouane, S. Guyard, É. Larquet, and J.-P. Contour, Phys. Status Solidi A **203**, 2209 (2006).
[58] F. J. Wong, S.-H. Baek, R. V. Chopdekar, V. V. Mehta, H.-W. Jang, C.-B. Eom, and Y. Suzuki, Phys. Rev. B **81**, 161101(R) (2010).
[59] S. Okamoto, A. J. Millis, and N. A. Spaldin, Phys. Rev. Lett. **97**, 056802 (2006).
[60] F. Schoofs, M. A. Carpenter, M. E. Vickers, M. Egilmez, T. Fix, J. E. Kleibeuker, J. L. MacManus-Driscoll, and M. G. Blamire, J. Phys. Condens. Matter **25**, 175005 (2013).
[61] T. T. Fister, H. Zhou, Z. Luo, S. S. A. Seo, S. O. Hruszkewycz, D. L. Proffit, J. A. Eastman, P. H. Fuoss, P. M. Baldo, H. N. Lee, and D. D. Fong, APL Mater. **2**, 021102 (2014).
[62] H. Rotella, U. Lüders, P.-E. Janolin, V. H. Dao, D. Chateigner, R. Feyerherm, E. Dudzik, and W. Prellier, Phys. Rev. B **85**, 184101 (2012).